frontiers | Frontiers in Earth Science

TYPE Original Research
PUBLISHED 20 January 2023
DOI 10.3389/feart.2023.1133539

OPEN ACCESS

EDITED BY
Jiyuan Yin,
Chinese Academy of Geologi-cal Sciences (CAGS), China

REVIEWED BY
Xiaochen Zhao,
Xi'an University of Science and Technology, China
Zhongnan Wang,
Research Institute of Petroleum Exploration and Development (RIPED), China

*CORRESPONDENCE
Aiguo Wang,
wag@nwu.edu.cn

SPECIALTY SECTION
This article was submitted to Petrology, a section of the journal Frontiers in Earth Science

RECEIVED 29 December 2022
ACCEPTED 12 January 2023
PUBLISHED 20 January 2023

CITATION
Yang Z, Wang A, Meng P, Chen M, Guo K and Zhu N (2023), Combined use of in-reservoir geological records for oil-reservoir destruction identification: A case study in the Jingbian area (Ordos Basin, China).
Front. Earth Sci. 11:1133539.
doi: 10.3389/feart.2023.1133539

Combined use of in-reservoir geological records for oil-reservoir destruction identification: A case study in the Jingbian area (Ordos Basin, China)

Zeguang Yang[1], Aiguo Wang[1]*, Pengyun Meng[2], Min Chen[2], Kai Guo[1] and Nan Zhu[1]

[1]State Key Laboratory of Continental Dynamics, Department of Geology, Northwest University, Xi'an, China, [2]No.1 Oil Production Plant of Changqing Oilfield Company, Yan'an, China

Rapid identification of reservoir destruction is critical to avoid exploration failure. More indicators of reservoir destruction are urgently needed to be developed besides the evaluation methods of trap effectiveness based on structural analysis. Here, we provide a case study in the Ordos Basin to show that the combined use of in-reservoir geological records is a robust tool to rapidly identify oil-reservoir destruction. The sandstones within the Yanchang Formation in the oil-depleted Jingbian area were investigated by petrological and geochemical analysis. The results show that 1) the oils with increased density and viscosity occur in the low permeability sandstones, whereas the high permeability sandstones were occupied by water, 2) abundant solid bitumen occur in the intergranular pores, 3) the n-alkanes with carbon numbers less than 19 are significantly lost from the original oils, and 4) the majority of paleo oil layers have evolved into present water layers. All these in-reservoir physicochemical signatures unravel the same geological event (i.e., oil-reservoir destruction) in the Jingbian area. This oil-reservoir destruction was likely caused by the uplift-induced erosion and the fault activities after oil accumulation during the Late Early Cretaceous.

KEYWORDS

Ordos Basin, jingbian area, Yanchang Formation, oil-reservoir destruction, geological record

1 Introduction

Reservoir destruction is a common geological event (Beydoun, 1997; Fu et al., 2000; Gartrell et al., 2004; Pang et al., 2012; Isiaka et al., 2017; Wang W. Y. et al., 2019), and is extremely unfavorable to oil and gas exploration. In order to reduce exploration risks, it is necessary to carry out the reservoir destruction identification and assessment in the exploration area. Uplift-induced erosion and fault activity are considered to be the two main causes of reservoir destruction (e.g., Fu et al., 2000; Pang et al., 2018). Faulting activity (e.g., Gartrell et al., 2004; Isiaka et al., 2017; Palladino et al., 2020) and tectonic evolution (e.g., Pang et al., 2012; Wang W. Y. et al., 2019) were always studied through geological and geophysical methods to evaluate trap effectiveness in the previous studies. However, these structural analyses for reservoir destruction still need the supports from in-reservior evidences. In fact, tectonic uplift and fault activity can cause a series of secondary physicochemical and microbial alteration which occur within the reservoirs or the overlying strata, such as phase fractionation (e.g., Thompson, 1987; Meulbroek et al., 1998), water washing (e.g., Lafargue and Barker, 1988), biodegradation

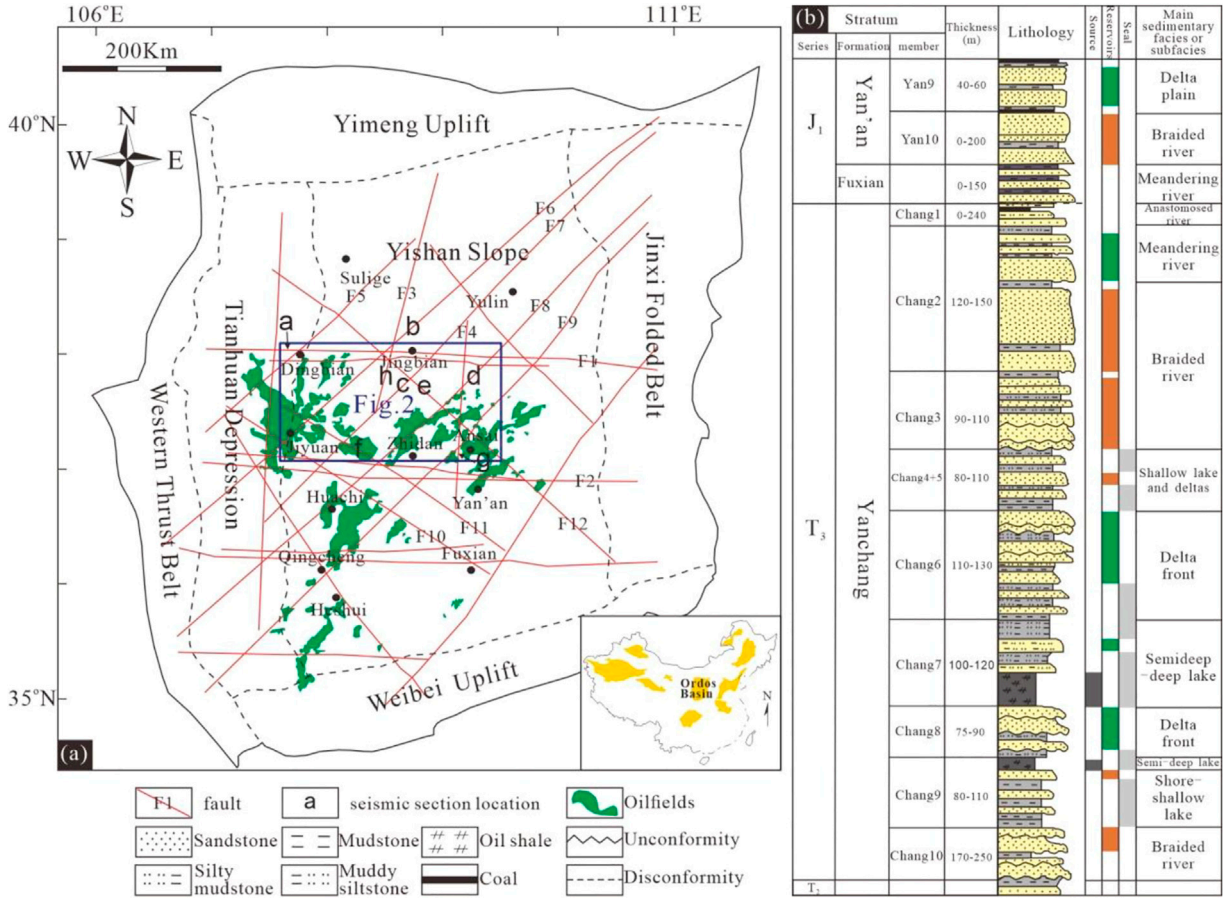

FIGURE 1
Tectonic units and oil-reservoir distribution **(A)** and Lithology, source rocks, reservoirs, seals and sedimentary facies of the Yanchang-Yan'an Formations **(B)** in the Ordos Basin (Modified from Hui et al., 2019; Qu et al., 2020; Wu, 2020; Yang et al., 2021).

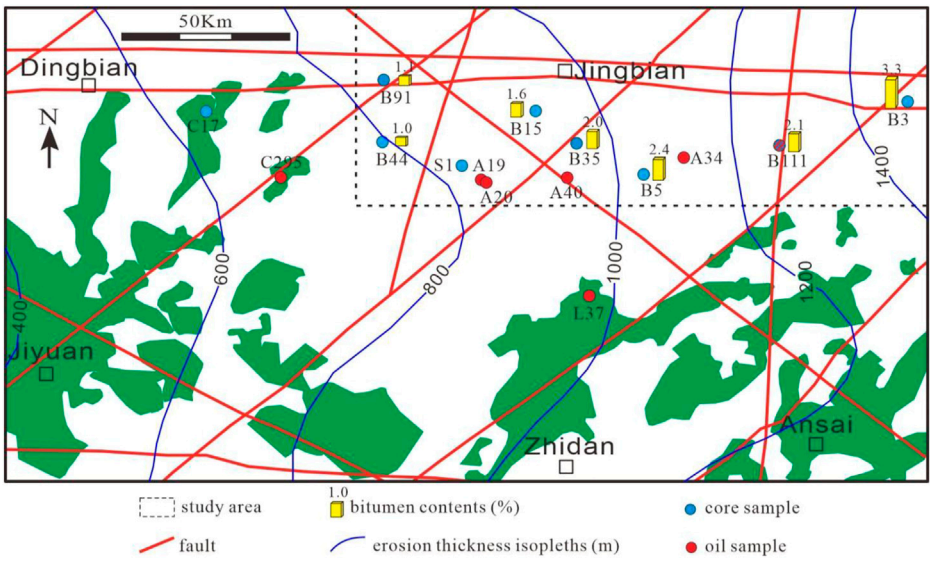

FIGURE 2
Distribution of oil-reserviors and sampling wells in the Jingbian and adjacent areas (erosion thickness during the Late Cretaceous according to Chen et al., 2006; fault distribution according to Wu, 2020).

(e.g.,Curiale and Bromley, 1996; Oldenburg et al., 2017), diagenetic alteration (Xie et al., 2021; Zhang et al., 2022) and surface oil/gas seepages. Such geological records are all potential indicators of reservoir destruction, and the combined use of them are expected to be powerful to rapidly identify reservoir destruction. Here, we provide a case study in the Ordos Basin to show the important role of in-reservoir geological records play in the identification of oil-reservoir destruction.

During the 40 years of petroleum exploration, 4 oil-enriched areas (OEA) have been founded in the central Ordos Basin (Figure 1A). Each of them contains oil reserves over 10×10^8t (Hui et al., 2019). The Jingbian area is adjacent to the Dingbian-Jiyuan OEA to the west and Zhidan-Ansai OEA to the south (Figure 1; Figure 2) but contains few oil resources. The cause of oil depletion in this area is still unclear, which has resulted in frequent exploration failure. In this study, the sandstone reservoirs in the Jingbian area were investigated through an integrated analysis including microscopic observation, laser Raman, whole-hydrocarbon gas chromatography, quantitative grain fluorescence (QGF) and QGF on extract (QGF-E). The aim of this study is to 1) identify the oil-reservoir destruction in the studied area, and 2) show the important role of in-reservoir geological records play in the identification of oil-reservoir destruction.

2 Geological setting

The Ordos Basin, which covers an area of about 36×10^4 km^2, is the second largest petroliferous basin in China, and produces more than 400 million barrels of oil equivalent per year (Hui et al., 2019). According to the diversity of basement structure, the basin is divided into six tectonic units, including Yimeng Uplift, Yishan Slope, Weibei Uplift, Western Thrust Belt, Tianhuan Depression, and Jinxi Folded Belt (Cui et al., 2019; Cui et al., 2022) (Figure 1A). The Yishan Slope, which contains the 4 OEAs, is now a west dipping monocline with an angle less than 1° (Xu et al., 2017). Within the slope, there exists six NE-SW trending, five NW-SE trending, four nearly E-W trending and two N-S trending faults (Figure 1A) (Wu, 2020).

The oil resources in the Ordos Basin are mainly stored in the Mesozoic petroleum system, including the Triassic Yanchang Formation and Jurassic Fuxian- Yan'an formations (Qu et al., 2020) (Figure 1B), which were deposited in fluvial-delta-lake sedimentary systems (Zhou et al., 2008; Qiu et al., 2015). Both of them are subdivided into 10 members, numbered from top to bottom as Chang 1 to Chang 10, and Yan 1 to Yan 10, respectively. The Chang 7 Member containing black organic-rich shale is the chief oil source (Cui et al., 2019), while the sandstones in the Yan 9, Chang 2, Chang 6, Chang 7 and Chang 8 members are the major reservoirs. Thick mudstone and shale layers in the two formations are the seals of underlying oil reservoirs (Figure 1B) (Qu et al., 2020).

The Ordos basin has experienced multiple tectonic movements since the Yanchang Formation was deposited. With the continent-continent collision of the Yangtze plate and North China plate during the late Triassic (Bao et al., 2020; Wu et al., 2020), the Ordos Basin was uplifted and underwent the erosion of the Chang 1 ~ Chang 3 members. Subsequently, the Fuxian and Yan'an formations unconformably covered the Yanchang Formation. During the middle to late Jurassic, the thrust-nappe belt in the western margin of the basin developed, leading to erosion in the middle and eastern basin with a maximum erosion thickness of 300 m (Chen et al., 2006). During the Early Cretaceous, the Ordos Basin subsided to maximum buried depth due to the movement of paleo-Pacific plate (Wu et al., 2020). During the Late Cretaceous to early-middle Eocene, the Ordos Basin experienced the strongest tectonic uplift, resulting in the erosion of the pre-Late Cretaceous. The erosion thicknesses in the Jingbian area vary from the 800 m–1400 m (Figure 2), and the maximum erosion thicknesses can be up to 1800–2000 m in the eastern basin (Liu et al., 2006). Since the Late Miocene, the Tibet Plateau uplift has caused the uplift in the west and subsidence in the east of the basin, forming the present tectonic framework (Ma et al., 2019).

The present exploration target in the Jingbian area and adjacent OEAs is the Chang 6 Member. Its burial depths vary from ~2500 m in the western Dingbian area to ~700 m in the eastern Jingbian area. The petrological characteristic and physical property of the Chang 6 reservoir are almost the same between the studied Jingbian area and adjacent OEAs, which is characterized by fine-medium grain (0.125–0.5 mm) arkose, dominated calcite/laumontite cements and low/ultra-low permeability (Wei et al., 2003; Hui et al., 2019; Ao et al., 2022).

3 Samples and methods

Twenty-five sandstone-reservoir samples and six crude oil samples were collected from the wells in the Jingbian area and adjacentDingbian-JiyuanOEAs (Figure 2). Gas chromatography was conducted on the crude oils using Trace 1300 system equipped with an HP-1 capillary column (30 m × 0.25 mm × 0.25 m). The temperatures of the sample inlet and FID detector are all 300°C. The temperature program was 40°C for 10 min, 40°C–70°C at 4°C/min, 70°C–300°C at 8°C/min, and finally held at 310°C for 40 min. Nitrogen was used as carrier gas at a flow rate of 1 mL/min.

Casting thin sections without cover glass and doubly polished thin sections for fluid inclusion were prepared for the observation of petrography and fluid inclusion under a ZEISS Axio Scope A1 microscope (with 100 W high-pressure mercury lamp). Coeval oil and aqueous inclusions in the doubly polished thin sections were examined on a THMS600 Linkam Heating and Freezing stage for homogenization temperatures (T_h). The analytical uncertainties are better than 0.1°C.

The burial and thermal history for single well was recovered through basin model 1D and constrained by the measured vitrinite reflectance at various depths. Lithology was determined by the cuttings logging and log data. The main parameters erosion thickness and geothermal gradient were cited from Chen et al. (2006) and Ren et al. (2017).

A HORIBA LabRAM Odyssey spectrometer was applied to identify the unrecognizable minerals in the casting thin sections through Raman spectral analysis. The measuring conditions are: laser wavelength 785 nm, exposure time 20 s, scanning wave number range 1000–2000 cm^{-1}, and superposition twice.

QGF is measured by fluorescence emission spectra from reservoir grains, after a cleaning procedure involving solvent, hydrogen peroxide and hydrochloric acid. QGF-E is measured by fluorescence emission spectra from the solvent extract from reservoir grains after the QGF cleaning procedure following Liu and Eadington (2005).

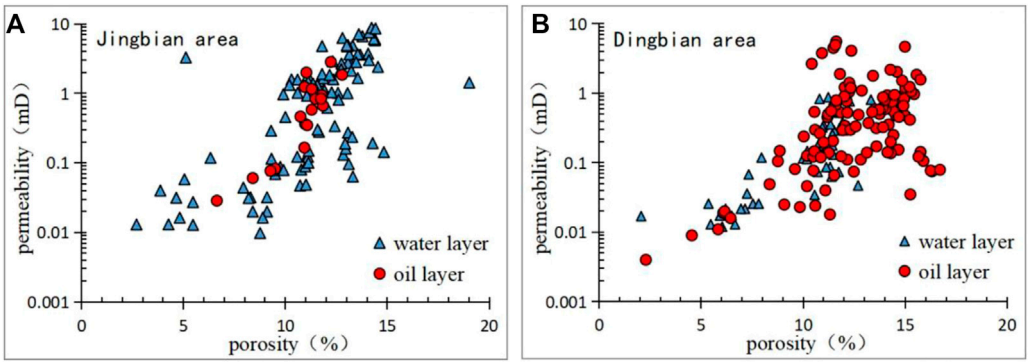

FIGURE 3
Porosity and permeability of oil/water layers in the Chang 6 Member in the Jingbian **(A)** and Dingbian **(B)** areas.

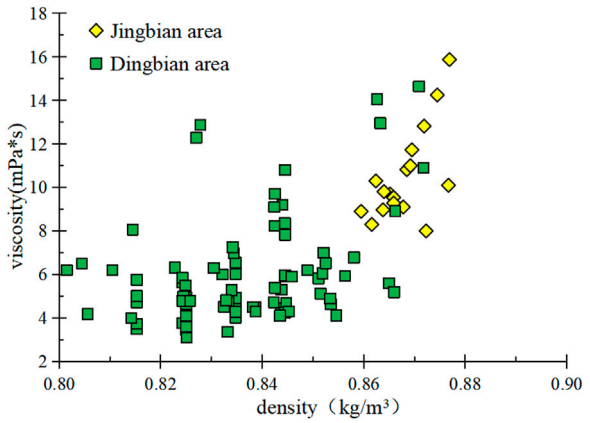

FIGURE 4
Density and viscosity of the Chang 6 oils in the Jingbian and Dingbian areas.

In addition, the physical properties of core and crude oils, as well as the formation testing data in the study area and adjacent areas were collected from the PetroChina Changqing Oilfield Company.

4 Results

4.1 Porosity-permeability of oil and water layers

The sandstone reservoirs were divided into oil layers and water layers based on the collected formation testing data. Subsequently, the measured core porosity-permeability corresponding to oil layers and water layers were respectively counted. The sandstone reservoirs in the study area and adjacent OEAs are both typical tight sandstone reservoir with significant heterogeneity (Wei et al., 2003; Hui et al., 2019; Ao et al., 2022), but the oil-bearing property is obviously different between them. As shown in Figure 3, the porosity and permeability ranges of oil layers in the Jingbian area are limited, mainly varying from 10% to 12%, and from 0.1 mD to 2 mD, respectively (Figure 3A). On the contrary, the water layers are characterized by much larger porosity-permeability ranges, including the high-quality sandstones with porosity greater than 12% (Figure 3A). However, in the adjacent Dingbian OEA, the oils mainly occur in the high-quality reservoirs with porosity greater than 10% and permeability greater than 0.1 mD, while the water occupies the sandstones with porosity and permeability respectively less than 12% and 1 mD (Figure 3B).

In summary, the present high-quality sandstones were occupied by water in the Jingbian area, but were occupied by oils in the adjacent OEA.

4.2 Density and viscosity of oils

As shown in Figure 4, the density of crude oils in the Jingbian area varies from 0.86 kg/m^3 to 0.88 kg/m^3, which are obviously heavier than the oils in the Dingbian area. The viscosity of crude oils in the Jingbian area varies from 8 mPa*s to 16 mPa*s, which are more viscous than the oils in the Dingbian area.

4.3 Solid bitumen

Microscopic observation shows that the majority of intergranular pores within the Chang 6 Member in the Jingbian area are filled by the black solid matters (Figures 5A, C). They are identified to be solid bitumen by the Raman spectra with the two first-order characteristic bands, i.e., the D band near 1380 cm^{-1} and G band near 1590cm^{-1} (Figures 5B, D) (Zerda et al., 1981).

According to the estimated solid bitumen content in each casting thin section, the solid bitumen abundance in the study area is shown (Figure 2). The solid bitumen content gradually increases from 1.0% in the west to 3.3% in the east. The average content of the whole study area is 2.1%.

4.4 N-alkane abundance distribution of oils

The abundance of n-alkane in primary maturated oils exponentially decreases as the carbon number increases (Kissin, 1987; Meulbroek et al., 1998). This pattern, however, can be broken by several geological processes (e.g., biodegradation and phase fractionation).

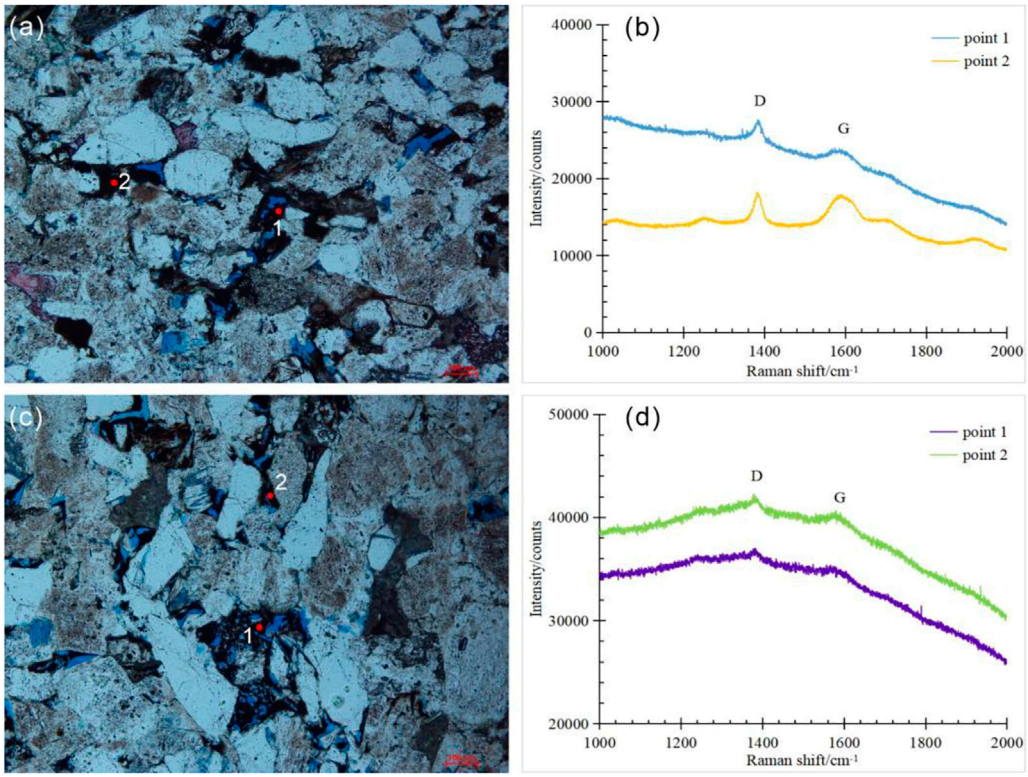

FIGURE 5
Solid bitumen occurrence in the reservoir and its Raman spectra (red points indicate Laser Raman testing location; **(A,B)** B111 well, 969.56 m, Chang 6 Member; **(C,D)** Q3 well, 719.15 m, Chang 6 Member).

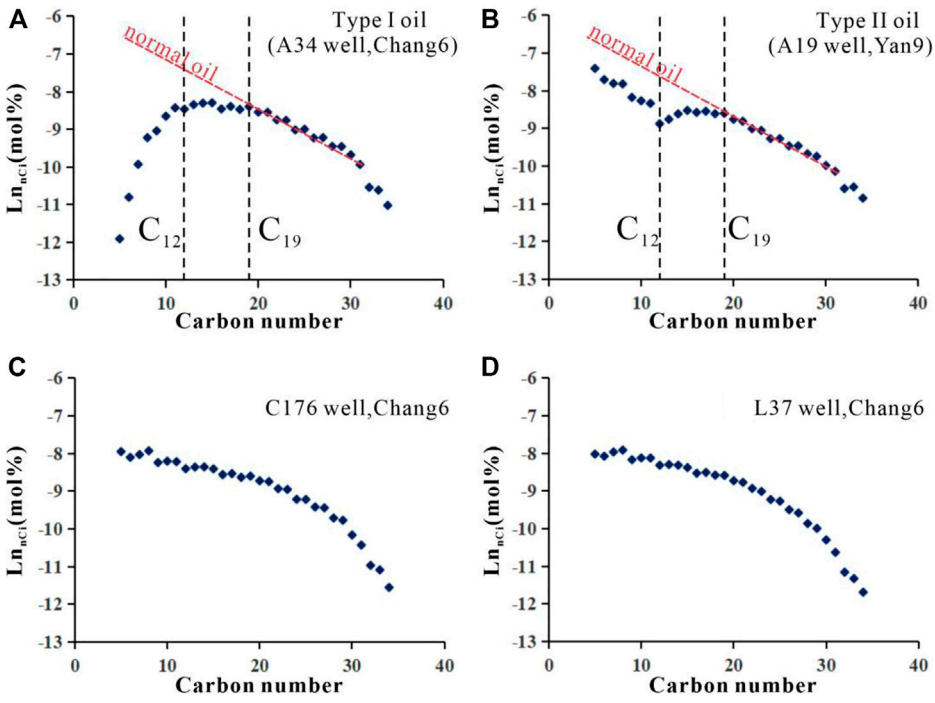

FIGURE 6
N-alkane abundance distributions of crude oils in the Jingbian and adjacent areas. **(A)**: oil with the n-alkane abundance negative deviation from the exponential pattern at C19, and the deviation degree obviously increases for the carbon numbers less than C12. **(B)**: oil with the n-alkane abundance negative deviation from the exponential pattern at C19, but the deviation degree decreases for the carbon numbers less than C12. **(C,D)**: oil with the n-alkane abundance approximate to exponential distribution.

TABLE 1 Geochemical parameters of crude oils in the Jingbian area and the adjacent OEAs.

Sample ID	Well	Formation	Pr/nC_{17}	Ph/nC_{18}	Tol/nC_7	nC_7/MCC_6	Q (%)
O1	B111	Chang 6	0.43	0.50	0.20	0.50	63.7
O2	A34	Chang 6	0.46	0.54	0.19	0.51	61.9
O3	A19	Yan 9	0.41	0.43	0.10	0.71	—
O4	A40	Yan 9	0.40	0.42	0.11	0.71	—
O5	C176	Chang 6	0.40	0.38	0.25	0.50	—
O6	L37	Chang 6	0.32	0.34	0.33	0.73	—

Abbreviations: Pr = pristine; nC_{17} = n-heptadecane; Ph = phytane; nC_{18} = n-octadecane; Tol =Toluene; nC_7 = heptane; MCC_6 = Methyl-cyclohexane; Q = light-end loss percentage.

TABLE 2 QGF & QGF-E data and identified results in the study area and adjacent areas.

Well	Depth m)	QGF index	QGF-E intensity (pc)	Paleo		Present	
				Oil layer	water layer	Oil layer	water layer
B5	1535.5	7.34	34.31		√		
	1539.83	12.17	59.82	√		√	
	1541.5	9.83	18.3		√		√
	1542.47	15.02	6.23	√			√
	1543.2	18.47	21.6	√			
B3	701	6.24	29.94		√		
	704.35	10.13	3.22				√
	708.6	18.92	31.02	√			
	715.4	12.4	40.21	√		√	
	718.6	18.7	41.23	√		√	
	722.8	29.37	5.22	√			√
	727	18.06	11.23	√			√
C17	1912.03	5.68	2.92		√		√
	1915.2	33.42	289.53	√		√	
	1916.95	19.8	51.62	√		√	
	1920.1	7.61	10.63		√		√
	1922.54	8.94	9.42		√		√
	1924.9	19.97	83.2	√		√	

The studied oils from the Chang 6 Member in the Jingbian area are characterized by a negative deviation from the exponential pattern at C_{19} (Figure 6A). The deviation degree obviously increases for the n-alkanes with carbon numbers less than C_{12} (nC_{12-}), indicating a significant nC_{12-} depletion. The n-alkanes of the oils from the overlying Yan'an Formation also deviate negatively at C_{19}, but the deviation degree decreases for the nC_{12-} (Figure 6B), indicating an nC_{12-} invasion into the nC_{19-} depleted oils. Notably, the oils from the adjacent OEAs display a pattern approximate to exponential distribution (Figures 6C, D), suggesting that they are mature and unaltered oils.

Based on the whole-hydrocarbon gas chromatography, the geochemical parameters for biodegradation: pristine/n-heptadecane (Pr/nC_{17}), phytane/n-octadecane (Ph/nC_{18}), and the parameters for phase fractionation: toluene/heptane (Tol/nC_7) and heptane/methylcyclohexane (nC_7/MCC_6) were calculated for further analysis (Table 1).

4.5 QGF & QGF-E

QGF & QGF-E is a set of fluorescence detection technology developed by Liu and Eadington (2005) and Liu et al. (2007) to detect the fluorescence of oil inclusions in clastic grains and adsorbed hydrocarbons on the surface of clastic grains. Two parameters, QGF

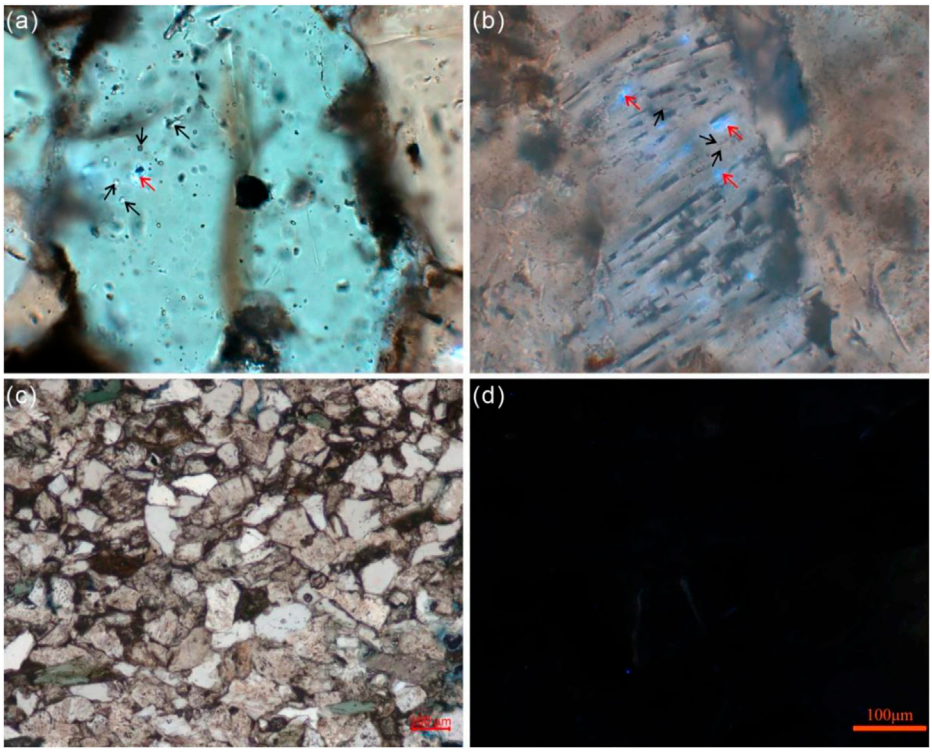

FIGURE 7
Micrographs of sandstones in the Jingbian area **(A)**. S1 well, 1890.48 m, Chang 7; **(B)**. B3 well, 709.9 m, Chang 6; **(C,D)**. B3 well, 704.35 m, Chang 6; the red and black arrows indicate oil and queous inclusions, respectively.

TABLE 3 T_h values of aqueous inclusions coeval with oil inclusions in the study area.

Well	Depth(m)	Formation	Hosting mineral	Occurrence	T_h (°C)
S1	1887.9	Chang 7	feldspar	healed intragranular pore	112.8
					110.3
	1889.06				113.3
	1890.48				112.3
					113.0
					109.9
B3	709.9	Chang 6	feldspar	healed intragranular pore	91.0
					89.4
					94.0
	706.9		quartz	healed fractures	93.2
					92.5
					87.4
					91.5

index and QGF-E intensity, were created to identify paleo- and present oil layers, respectively (Liu et al., 2007). The QGF index of core samples from the Chang 6 Member in the Jingbian area varies from 6.24 to 29.37 with an average of 14.72, while the QGF-E intensity ranges from 3.22 pc to 59.82pc, with an average of 25.19pc (Table 2).

4.6 Fluid inclusion

The coeval oil and aqueous inclusions in the sandstones in the Yanchang Formation in the Jingbian area have been observed (Figures 7A, B). The oil inclusions were trapped within healed secondary

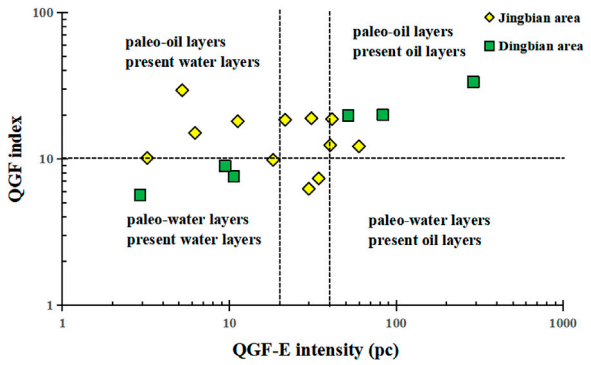

FIGURE 8
Cross plot of QGF index and QGF-E intensity in the Jingbian and Dingbian areas.

fractures in quartz and intragranular pore in feldspar grains, and exhibit bluish-white fluorescence. The T_h values of aqueous inclusions coeval with oil inclusions in the western and eastern parts of Jingbian area are 109.9–113.3°C and 87.4–94.0°C respectively (Table 3).

5 Discussion

5.1 Oil accumulation in the Jingbian area

Undoubtedly, solid bitumen is an indicator of oil charging (Littke et al., 1996; Huc et al., 2000; Liu et al., 2009). Wang et al. (2006) suggested that the reservoir with solid bitumen content greater than 2.0% can be defined as a paleo-oil reservoir. Solid bitumen is widely distributed in the study area (Figure 2), and 57% core samples contain the solid bitumen content greater than 2.0%, indicating that the Jingbian area, like the adjacent OEAs, is also a favorable area for oil accumulation.

QGF & QGF-E is widely used in the reconstruction of reservoir evolution (Wang et al., 2017; Liu et al., 2019; Song et al., 2022). According to the previous experience (Liu and Eadington, 2005; Liu et al., 2007), the QGF index of paleo-oil layers are generally greater than 4, and those of paleo-water layers are generally less than 4; The QGF-E intensity of present oil layers are generally greater than 40pc, while those of present water layers are generally less than 20pc. If the experiential QGF index is applied to the Jingbian area, all the studied core samples will be identified as paleo-oil layers.

The developer of QGF & QGF-E emphasized that the identification standards for paleo (present) oil (water) layers should be in line with local conditions (Liu and Eadington, 2005; Liu et al., 2007). According to the comparison between the QGF&QGF-E values and core observation, microscopic observation and formation testing results, the experiential QGF-E intensity ranges for identifying present oil/water layer are still applicable in the Jingbian area. However, the experiential QGF index value for distinguishing paleo oil/water layer is not effective anymore. Take the sandstone at 704.35 m of B3 well for example, its QGF index is 10.13, and will be classified into paleo oil layer according to the experiential standard. In fact, this sandstone is characterized by water wetting, 5.3% matrix content, strong compaction (linear contact among clastic grains), little bitumen (Figure 7C), few cements and no fluorescence (Figure 7D), which suggests that the subsurface fluids including oil have not charged this sandstone at all. Eventually, the QGF index boundary between paleo-oil and water layers in the study area is suggested as 10.13.

According to the QGF index and QGF-E intensity, the paleo- and present oil/water layers were identified (Figure 8; Table 2). Of 12 reservoir samples in the Jingbian area, 8 samples (accounting for 67%) belong to paleo-oil layers, showing that the large scale of oil accumulation have ever occurred in the study area.

The time of oil accumulation is determined using the T_h values of fluid inclusion and burial-thermal history (Figure 9). The T_h values of aqueous inclusions coeval with oil inclusions in the Chang 7 reservoir of S1 well range from 109.9°C to 113.3°C, while those in the Chang 6 reservoir of B3 well range from 87.4°C to 94.0°C (Table 3). These two T_h ranges plotting within the burial-thermal histories in the S1 and B3 wells both indicate that the oil accumulation occurred during the Late Early Cretaceous, prior to the tectonic uplift of the Ordos Basin during the Late Cretaceous (Figure 9).

5.2 Oil-reservoir destruction

As mentioned above, oils have accumulated during the Late Early Cretaceous in the Jingbian area. However, no commercial oil pools have been found now, which is likely attributed to paleo-oil reservoir destruction based on the following in-reservoir geological evidences.

5.2.1 Evolution from paleo-oil layers into present water layers

QGF & QGF-E provides direct evidence for the paleo-oil reservoir destruction occurred in the Jingbian area. Take B5 well with thick-bedded sandstones in the Chang 6 Member for example, the sandstones are dominated by water layers and oil-water layers, consistent with the results indicated by QGF-E intensity (Figure 10A). The QGF index, however, indicate that the oil-water layer in the lower part was an oil layer before (Figure 10A). This evolution from paleo oil layers into present water layers is more obvious in B3 well. The most majority of sandstones in Figure 10B were paleo oil layers, but now are dominated by water layers and oil-water layers. Overall, of the 8 samples identified as paleo oil layer, 3 samples are identified as present oil layer (Figure 8; Table 2), indicating that 62.5% of paleo oil layers have been destructed and evolved into present water layers.

In comparison, the QGF & QGF-E values in the Dingbian OEA show that the samples that were identified as paleo oil layer were also identified as present oil layer (Figure 8 and Figure 10C), indicating that the paleo oil reservoirs in the Dingbian area have not been destructed yet. That is why the oils are enriched there now.

5.2.2 Light fraction loss of oils

The n-alkane abundance distribution pattern of oils also provides the evidence for paleo oil-reservoir destruction. As shown in Figures 6A, B, the oils in the study area are characterized by the loss and invasion of light fraction. To explain this, we have carefully considered several geological processes and sampling process that may affect the oil compositions. Organic molecules tend to be degraded at different rates due to different resistance to biodegradation (Bennett et al., 2013;

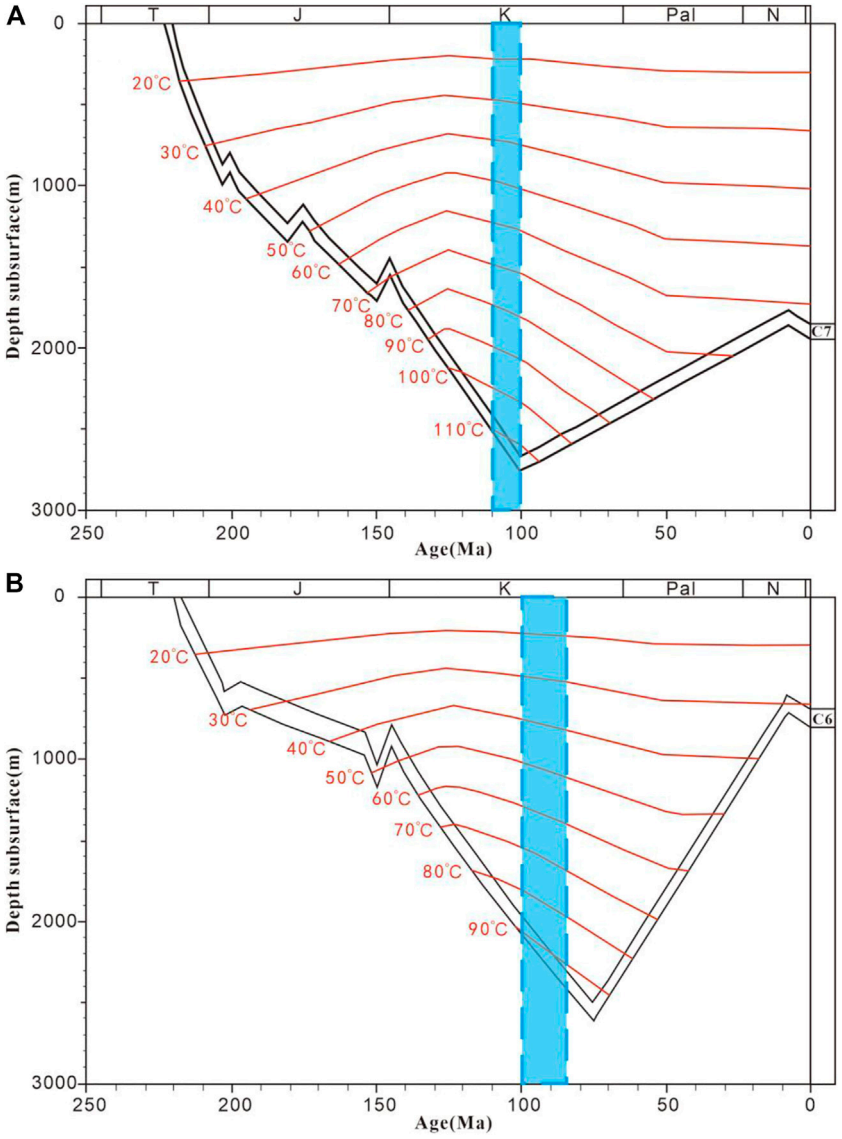

FIGURE 9
Oil accumulation time determined by T_h vales and burial-thermal history in S1 **(A)** and B3 **(B)** wells in the Jingbian area (C6= Chang 6 Member; C7=Chang 7 Member).

Wang et al., 2013). The first indications of oil biodegradation typically occurred with the selective removal of normal alkanes. As biodegradation proceeded, normal alkanes are degraded faster than mono- and multi-methylated alkanes (Peters et al., 2005). Thus, biodegradation can be ruled out due to a full range of n-alkanes observed in the oils and normal Pr/nC_{17} and Ph/nC_{18} values (Table 1). Water washing was also ruled out because the oils contain significant amounts of toluene (Table 1) (Napitupulu et al., 2000). Paraffin precipitation only affects n-alkanes at high carbon number end (e.g., >30, Losh et al., 2002). Fractionation in the separator and short term evaporation of samples after collection have been shown by Meulbroek et al. (1998) to affect the compounds as heavy as decane. Instead, evaporative fractionation is the most likely cause for the n-alkane distribution patterns of the studied oils based on the two facts: 1) the Chang 6 oils have lost the nC_{12-} which are exact the compositions invading into the overlying Yan 9 oils in the Jingbian area, and 2) the Tol/nC_7 values of Chang 6 oils are greater than those of Yan 9 oils, while the nC_7/MCC_6 values of Chang 6 oils are less than those of Yan 9 oils.

The evaporative fractionation resulted in the upward migration of light-end compositions originating from the Chang 6 Member, which is expected to have caused oil-reservoir destruction in the study area. According to the calculation method proposed by Losh et al. (2002), the light-end loss percentage are 63.66% and 61.91% for the two residual oils (Table 1; Figure 11), indicating that the original oil-reservoirs have lost more than half of oil compositions. In the adjacent OEAs, however, the Chang 6 oils show little compositional loss (Figures 6C, D), suggesting that the oil-reservoirs there have not been destructed yet.

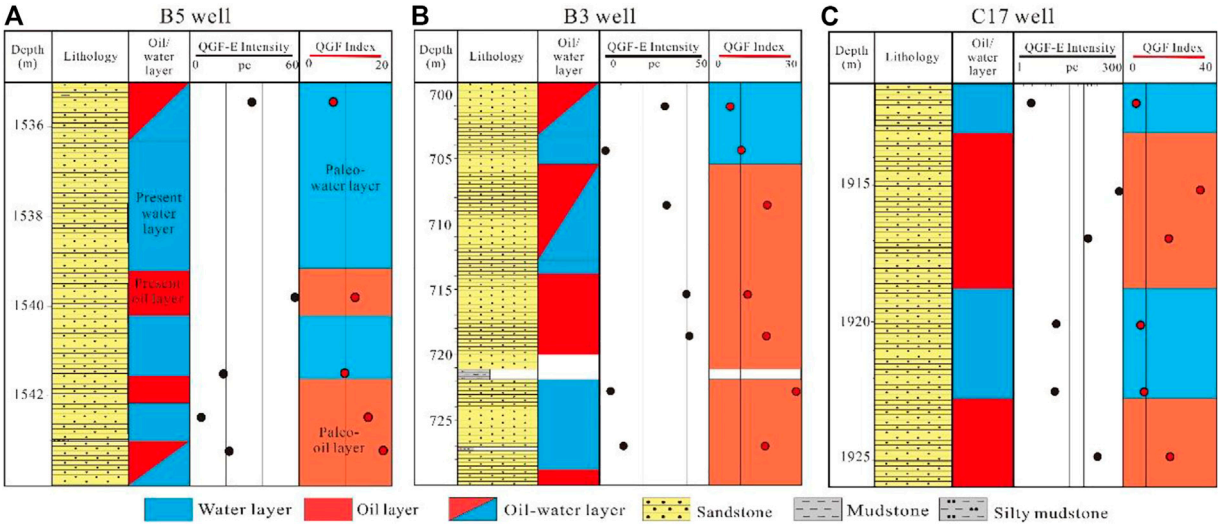

FIGURE 10
Paleo oil/water layers and present oil/water layers in the Chang 6 members of B5 well **(A)**, B3 well **(B)** in the Jingbian area and C17 well **(C)** in the adjacent Dingbian area.

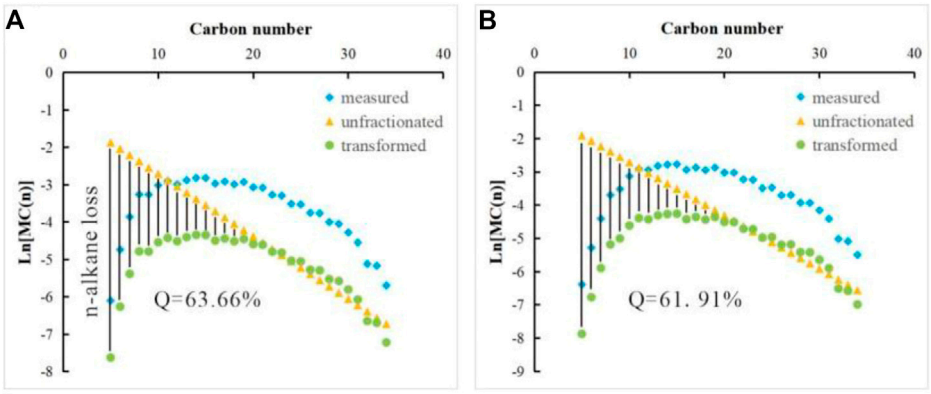

FIGURE 11
N-alkanes loss percentage of the studied oils **(A)** B111 well, Chang 6 Member; **(B)** A34 well, Chang 6 Member).

5.2.3 Elevated density-viscosity of oils and enrichment of solid bitumen

The density and viscosity of oils are controlled by the temperature, pressure and its chemical composition (Morales-Medina and Guzman, 2012; Said et al., 2016). The oils in the Yishan Slope mainly originated from the black shales in the Chang 7 Member in the central basin and accumulated during the Late Early Cretaceous (Hui, et al., 2019). Thus, the initial chemical compositions of these oils are expected to be similar. Under the same experimental conditions (20°C, 1atm), the elevated density-viscosity of oils suggests the occurrence of oil-reservoir destruction in the Jingbian area. Continuous compositional loss of light-end fraction during the oil-reservoir destruction will inevitably lead to the relative increase of heavy-end fraction in residual oils and finally form solid bitumen (Wang A. G. et al., 2019). It is should be noted that the density and viscosity of oils in the Jingbian area are obviously greater than those in the Dingbian OEA (Figure 5) and the solid bitumen are indeed more abundant in the Jingbian area (Figure 2; Figures 5A, C).

5.2.4 Oil occurrence in low-quality rather than high-quality reservoirs

Migrating oils tend to preferentially occupy the porosity with the lower capillary resistance (i.e., high porosity and permeability portions) after charging into the reservoirs. With the increase of oil saturation in trap, oils have to charge into the low porosity and permeability portions (England et al., 1987). Take the adjacent Dingbian OEA for example, oils are indeed occupying the high porosity and permeability reservoirs (Figure 3B).

On the other hand, when the oil-reservoirs were destructed, the oils in high porosity and permeability portions preferentially migrate out the trap, whereas the oils in low porosity and permeability portions were most likely left due to poor liquidity. In the Jingbian area, the sandstone reservoirs with high porosity and permeability are occupied by water, whereas the oils occur in the sandstone reservoirs with relative low porosity and permeability (Figure 3A). These oil-bearing characteristics in the Jingbian area are exactly consistent with the above oil/water behaviors caused by oil-reservoir destruction.

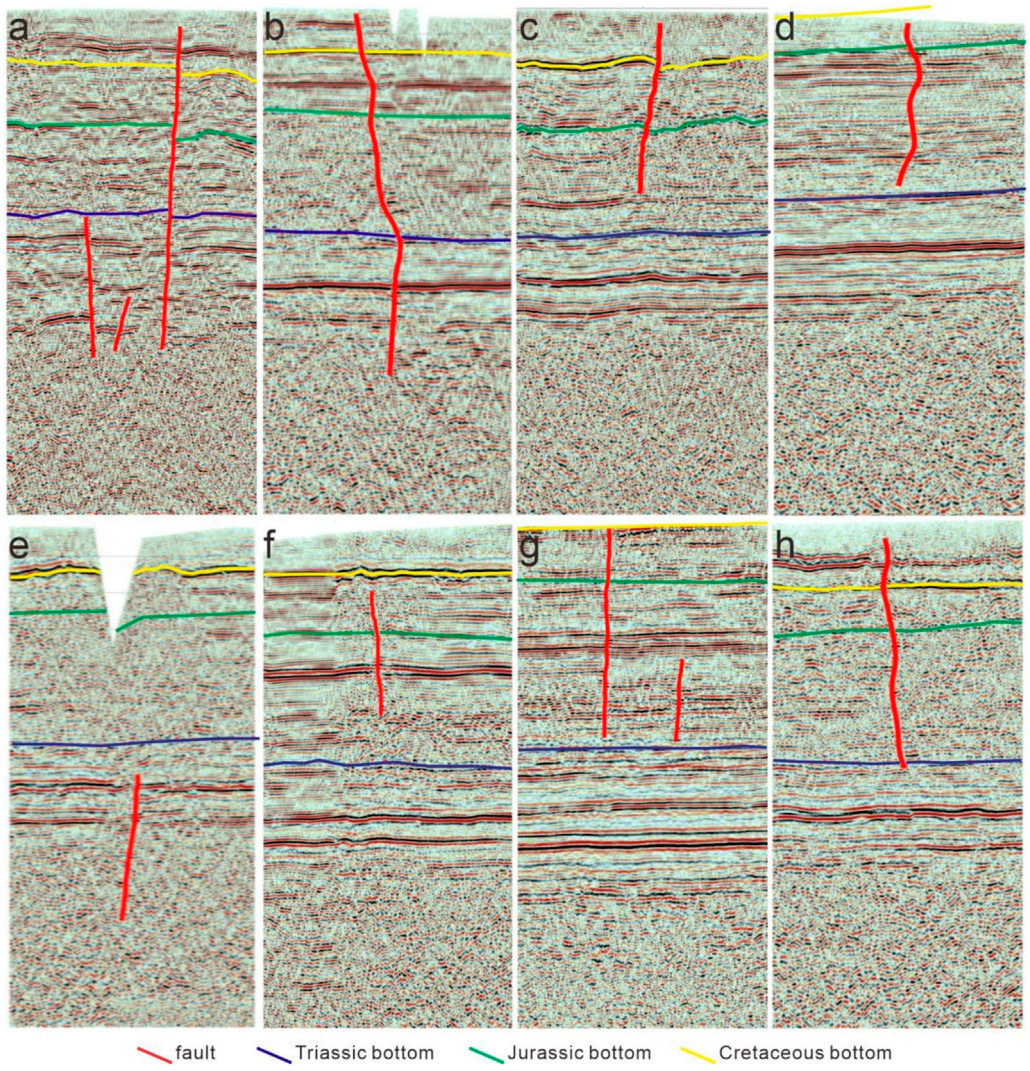

FIGURE 12
Seimic interpretation sections in the Jingbian and adjacent areas (modified from Wu, 2020). **(A)**: F1 fault. **(B)**: F6 fault. **(C)**: F7 fault. **(D)**: F8 fault. **(E)**: F12 fault. **(F)**: F11 fault. **(G)**: F4 fault. **(H)**: F3 fault.

5.3 Cause of oil-reservoir destruction

As mentioned above, uplift-induced erosion and fault activity were considered to be the two main causes of reservoir destruction (Fu et al., 2000; Pang et al., 2018), which should be responsible for the oil-reservoir destruction in the Jinbian area.

Since the oil accumulation during the Late Early Cretaceous, the Ordos Basin has experienced a long-period tectonic uplift from the Late Creataceous to Early-Middle Eocene. This tectonic uplift caused intense erosion with the erosion thickness increasing from west to east (Liu et al., 2006). In the study area, the erosion thicknesses vary from 800m to 1400 m (Figure 2) (Chen et al., 2006), generating a unconformity between the Middle Jurassic and Quaternary. Compared with the Dingbian OEA to the west, the uplift-induced erosion in the Jingbian area is more intense, which maybe has degraded the sealing of oil-reservoir and caused the oil-reservoir destruction in the area.

The Ordos Basin used to be considered as a stable cratonic basin with undeveloped faults. In recent years, however, multiple basement faults and concealed faults have been reported in the basin (Liu et al., 2013; Wu, 2020). There exist two E-W trending (F1, F2), two N-S trending (F3, F4), five NE-SW trending (F5-F9) and three NW-SW trending (F10-F12) faults in the Jingbian and adjacent areas (Figure 1A and Figure 2) (Wu, 2020). According to the seismic sections (Figure 12; Wu, 2020), the faults that cut across the Cretaceous (e.g., Figure Figures 12A–H) were likely active during the uplift and maybe have caused the oil-reservoir destruction. The faults that do not cut across the Cretaceous (e.g., Figures Figures 12E, F) were not active during the Cretaceous, and are thus not responsible for the oil-reservoir destruction. Overall, all the faults in the Jingbian and adjacent areas are likely active during the uplift, except the NW-SE trending faults. As shown in Figure 1A, there exist six potential faults (i.e., F1, F3, F4, F6, F7, and F8) for oil-reservoir destruction across the Jingbian area, whereas there exist two potential faults (i.e., F5 and F6) and three potential faults (i.e., F4, F8 and F9) in the Dingbian-Jiyuan OEA and Zhidan-Ansai OEA, respectively. Thus, the faults in the Jingbian area are more developed than those in the OEAs.

In summary, the tectonic uplift during the Late Cretaceous has caused uplift-induced erosion and fault activities, which likely further

caused the oil-reservoir destruction in the Jingbian area. In comparison, uplift-induced erosion and fault activities in the Dingbian and Ansai OEAs are relatively undeveloped, which is thus favorable for oil-reservoir preservation.

6 Conclusion

The Jingbian area in the Ordos Basin was used as a case to demonstrate that combined use of in-reservoir geological records is a robust tool to rapidly identify oil-reservoir destruction. The following conclusions were obtained from this study:

The Jingbian area is also a favorable area for oil accumulation, which occurred during the Late Early Cretaceous. The uplift-induced erosion and fault activities during the Late Cretaceous degraded the sealing of the oil-reservoir, and led to the oil-reservoir destruction. This process has been recorded by a series of geological signals in reservoirs, including 1) the loss of light fraction, 2) the increases of oil density and viscosity, 3) the enrichment of solid bitumen, 4) the evolution from paleo oil layers into current water layers, and 5) the oil occurrence in low-quality rather than high-quality reservoirs. These in-reservoir geological records provide a new technical approach for the oil-reservoir destruction identification.

Data availability statement

The original contributions presented in the study are included in the article/supplementary material, further inquiries can be directed to the corresponding author.

Author contributions

ZY, writing, mapping, experiment; AW, supervision, writing; PM, data collection, sampling, writing; MC, data collection, sampling, writing; KG, Sample preparation and editing; NZ, sample Sample preparation and polishing.

Funding

This work was supported by the National Natural Science Foundation of China (No.41402115); the Natural Science Basic Research Program of Shaanxi (2020JQ-591).

Conflict of interest

PM and MC were employed by No.1 Oil Production Plant of Changqing Oilfield Company

The remaining author declares that the research was conducted in the absence of any commercial or financial relationships that could be construed as a potential conflict of interest.

Publisher's note

References

Ao, C., Cheng, Y. H., Tang, Y. H., Wang, S. Y., Teng, X. M., Jin, R. S., et al. (2022). Detrital zircon analysis of the mesozoic strata in the northern Ordos Basin: Revealing the source-to-sink relationships and tectonic settings. *Geol. J.* 57, 3251–3266. doi:10.1002/gj.4472

Bao, H. P., Guo, W., Liu, G., Li, L., Wu, C. Y., and Bai, H. F. (2020). Tectonic evolution in the southern Ordos block and its significance in the tectono-depositional differentiation in the interior of the Ordos Basin. *Chin. J. Geol.* 55, 703–725. (in Chinese with English abstract). doi:10.12017/dzkx.2020.043

Bennett, B., Adams, J., Gray, N., Sherry, A., Oldenburg, T., Huang, H., P., et al. (2013). The controls on the composition of biodegraded oils in the deep subsurface - Part 3. The impact of microorganism distribution on petroleum geochemical gradients in biodegraded petroleum reservoirs. *Org. Geochem.* 56, 94–105. doi:10.1016/j.orggeochem.2012.12.011

Beydoun, Z. (1997). Prehistoric, ancient and mediaeval occurrences and uses of hydrocarbons in the greater Middle East region. *J. Pet. Geol.* 20, 91–95. doi:10.1111/j.1747-5457.1997.tb00757.x

Chen, R. Y., Luo, X. R., Chen, Z. K., Wang, Z. M., and Zhou, B. (2006). Estimation of denudation thickness of mesozoic stata in the Ordos Basin and its geological significance. *Acta Geol. Sin.* 05, 685–693. (in Chinese with English abstract).

Cui, J. W., Zhu, R. K., Li, S., Qi, Y. L., Shi, X. Z., and Mao, Z. G. (2019). Development patterns of source rocks in the depression lake basin and its influence on oil accumulation: Case study of the Chang 7 member of the triassic Yanchang Formation, Ordos Basin, China. *Nat. Gas. Geosci.* 4, 191–204. doi:10.1016/j.jnggs.2019.08.002

Cui, J. W., Zhang, Z. Y., Zhang, Y., Liu, G. L., and Qi, Y. L. (2022). Oil and gas accumulation periods and charging path of continental lake basin: A case study of the Chang 9-chang 10 oil reservoir in the Yanchang Formation in the Ordos Basin. *J. Pet. Sci. Eng.* 219, 111136–136. doi:10.1016/j.petrol.2022.111136

Curiale, J., and Bromley, B. (1996). Migration induced compositional changes in oils and condensates of A single field. *Org. Geochem.* 24, 1097–1113. doi:10.1016/S0146-6380(96)00099-X

England, W., Mackemzie, A., Mann, D., and Quigley, T. (1987). The movement and entrapment of petroleum fluids in the subsurface. *J. Geol. Soc.* 144, 327–347. doi:10.1144/gsjgs.144.2.0327

Fu, G., Fu, X. F., Xue, Y. C., and Yang, M. (2000). Analysis on geological factors causing the destroy and redistribution of oil and gas reservoirs. *Nat. Gas. Geosci.* 11, 1–7. (in Chinese with English abstract).

Gartrell, A., Zhang, Y., Lisk, M., and Dewhurst, D. (2004). Fault intersections as critical hydrocarbon leakage zones: Integrated field study and numerical modelling of an example from the timor sea, Australia. *Mar. Pet. Geol.* 21, 1165–1179. doi:10.1016/j.marpetgeo.2004.08.001

Huc, A. Y ., Nederlof, P., Debarre, R., Carpentier, B., Boussafir, M., Laggoun, F., et al. (2000). Pyrobitumen occurrence and formation in a cambro–ordovician sandstone reservoir, fahud salt basin, North Oman. *Chem. Geol.* 168, 99–112. doi:10.1016/S0009-2541(00)00190-X

Hui, X., Zhao, Y. D., Shao, X. Z., Zhang, W. X., Cheng, D. X., and Luo, A. X. (2019). The geological conditions, resource potential, and exploration direction of oil in Ordos Basin. *Mar. Orig. Pet. Geol.* 24, 14–22. (in Chinese with English abstract). doi:10.3969/j.issn.1672-9854.2019.02.002

Isiaka, A., Durrheim, R., Manzi, M., and Andreoli, M. (2017). 3D seismic analysis of the ak fault, orange basin, south Africa: Implications for hydrocarbon leakage and offshore neotectonics. *Tectonophysics* 721, 477–490. doi:10.1016/j.tecto.2017.10.011

Kissin, Y. (1987). Catagenesis and composition of petroleum: Origin of N-alkanes and isoalkanes inpetroleum crudes. *Geochim. Cosmochim. Ac.* 51, 2445–2457. doi:10.1016/0016-7037(87)90296-1

Lafargue, E., and Barker, C. (1988). Effect of water washing on crude oil composition. *AAPG Bull.* 73, 263–276. doi:10.1306/703C8C13-1707-11D7-8645000102C1865D

Littke, R., Brauckmann, F. J., Radke, M., and Schaefer, R. G. (1996). Solid bitumen in rotliegend gas reservoirs in northern Germany: Implications for their thermal and filling history. *Geol. Palaont. Teil.* 11, 1275–1292.

Liu, C. Y., Zhao, H. G., Gui, X. J., Yue, L. P., Zhao, J. F., and Wang, J. Q. (2006). Space—Time coordinate of the evolution and reformation and mineralization response in Ordos Basin. *Acta Geol. Sin.* 80, 617–638. (in Chinese with English abstract).

Liu, K., Eadington, P., Middleton, H., Fenton, S., and Cable, T. (2007). Applying quantitative fluorescence techniques to investigate petroleum charge history of sedimentary basins in Australia and Papuan New Guinea. *J. Pet. Sci. Eng.* 57, 139–151. doi:10.1016/j.petrol.2005.11.019

Liu, D., Xiao, X., Tian, H., Yang, C., Hu, A., and Song, Z. G. (2009). Identification of natural gas origin using the characteristics of bitumen and fluid inclusions. *Pet. explor. Dev.* 36, 375–382.

Liu, Z., Yao, X., Hu, X., D., and Wang, Q. (2013). Discovery of the mesozoic fault and its implication on the hydrocarbon accumulation in Ordos Basin. *J. Earth Sci. Environ.* 35, 56–66. (in Chinese with English abstract).

Liu, B., Bai, L., H., Chi, Y., A., Jia, R., Fu, X., F., and Yang, L. (2019). Geochemical characterization and quantitative evaluation of shale oil reservoir by two-dimensional nuclear magnetic resonance and quantitative grain fluorescence on extract: A case study from the qingshankou Formation in southern songliao basin, northeast China. *Mar. Pet. Geol.* 109, 561–573. doi:10.1016/j.marpetgeo.2019.06.046

Liu, K., and Eadington, P. (2005). Quantitative fluorescence techniques for detecting residual oils and reconstructing hydrocarbon charge history. *Org. Geochem.* 36, 1023–1036. doi:10.1016/j.orggeochem.2005.02.008

Losh, S., Cathles, L., and Meulbroek, P. (2002). Gas washing of oil along a regional transect, offshore Louisiana. *Org. Geochem.* 33, 655–663. doi:10.1016/S0146-6380(02)00025-6

Ma, X. J., Liang, J. W., Li, J. X., Jia, W. H., Tao, W. X., Liu, Y. L., et al. (2019). Meso-cenozoic tectonic uplift and evolution of central and western Ordos basin. *Northwest. Geol.* 52, 127–136. (in Chinese with English abstract). doi:10.19751/j.cnki.61-1149/p.2019.04.011

Meulbroek, P., Cathles, L., and Whelan, J. (1998). Phase fractionation at south eugene island block 330. *Org. Geochem.* 29, 223–239. doi:10.1016/S0146-6380(98)00180-6

Morales-Medina, G., and Guzman, A. (2012). Prediction of density and viscosity of Colombian crude oils from chromatographic data. *Ct&F - Cienc. Tecnol. Y Futuro* 4, 57–73.

Napitupulu, H., Ellis, L., and Mitterer, R. (2000). Post-generative alteration effects on petroleum in the onshore northwest java basin, Indonesia. *Org. Geochem.* 31, 295–315. doi:10.1016/S0146-6380(99)00154-0

Oldenburg, T., Jones, M., Huang, H., Bennett, B., Shafiee, N. S., Head, I. M., et al. (2017). The controls on the composition of biodegraded oils in the deep subsurface- Part 4. Destruction and production of high molecular weight non-hydrocarbon species and destruction of aromatic hydrocarbons during progressive in-reservoir biodegradation. *Org. Geochem.* 114, 57–80. doi:10.1016/j.orggeochem.2017.09.003

Palladino, G., Rizzo, R. E ., Zvirtes, G., Grippa, A., Philipp, R. P., Healy, D., et al. (2020). Multiple episodes of sand injection leading to accumulation and leakage of hydrocarbons along the san andreas/san gregorio fault system, California. *Mar. Pet. Geol.* 118, 104431. doi:10.1016/j.marpetgeo.2020.104431

Pang, H., Chen, J., Pang, X., Liu, K., and Xiang, C. (2012). Estimation of the hydrocarbon loss through major tectonic events in the tazhong area, tarim basin, west China. *Mar. Pet. Geol.* 38, 195–210. doi:10.1016/j.marpetgeo.2011.11.006

Pang, X., Jia, C., Pang, H., and Yang, H. (2018). Destruction of hydrocarbon reservoirs due to tectonic modifications: Conceptual models and quantitative evaluation on the tarim basin, China. *Mar. Pet. Geol.* 91, 401–421. doi:10.1016/j.marpetgeo.2018.01.028

Peters, K., Walters, C., and Moldowan, J. (2005). *The biomarker guide*. Editors K. E. Peters, C. C. Walters, and J. M. Moldowan (Cambridge, Uk: Cambridge University Press), 2, 490. Isbn 0521781582. The Biomarker Guide. doi:10.1017/CBO9780511524868

Qiu, X. W., Liu, C. Y., Mao, G. Z., Deng, Y., Wang, F. F., and Wang, J. Q. (2015). Major, Trace and platinum-group element geochemistry of the upper triassic nonmarine hot shales in the Ordos Basin, central China. *Appl. Geochem.* 53, 42–52. doi:10.1016/j.apgeochem.2014.11.028

Qu, H. J., Yang, B., Gao, S. L., Zhao, J. F., Han, X., Chen, S., et al. (2020). Controls on hydrocarbon accumulation by facies and fluid potential in large-scale lacustrine petroliferous basins in compressional settings: A case study of the mesozoic Ordos Basin, China. *Mar. Pet. Geol.* 122, 104668. doi:10.1016/j.marpetgeo.2020.104668

Ren, Z., Yu, Q., Cui, J. P., Qi, K., Chen, Z. J., Cao, Z. P., et al. (2017). Thermal history and its controls on oil and gas of the Ordos Basin. *Earth Sci. Front.* 24, 137–148. doi:10.13745/j.esf.2017.03.012

Said, S., Aboul-Fotouh, T., and Ashour, I. (2016). A current viscosity of different Egyptian crude oils: Measurements and modeling over A certain range of temperature and pressure. *J. Petroleum Environ. Biotechnol.* 7. doi:10.4172/2157-7463.1000305

Song, J., Chen, T., and Zhang, J. (2022). Permian and triassic hydrocarbon migration and accumulation in the cainan area, junggar basin, China. *J. Pet. Sci. Eng.* 210, 109965. doi:10.1016/j.petrol.2021.109965

Thompson, K. F. M. (1987). Fractionated aromatic petroleums and the generation of gas-condensates. *Org. Geochem.* 11, 573–590. doi:10.1016/0146-6380(87)90011-8

Wang, F. Y., Shi, Y. L., Zeng, H. S., and Liu, K. Y. (2006). To identify paleo-oil reservoir and to constrain petroleum charging model using the abundance of oil inclusions. *Bull. China Soc. Mineral. Pet. Geochem.* 25, 12–18.

Wang, G., Wang, T. G., Simoneit, B. R. T., and Zhang, L. (2013). Investigation of hydrocarbon biodegradation from A downhole profile in bohai bay basin: Implications for the origin of 25-norhopanes. *Org. Geochem.* 55, 72–84. doi:10.1016/j.orggeochem.2012.11.009

Wang, C., Zeng, J., Wang, F., Lin, X., Y., Liu, X., F., Wang, F., F., et al. (2017). Utility of GOI, QGF, and QGF-E for interpreting reservoir geohistory and oil remigration in the hudson Oilfield, tarim basin, northwest China. *Mar. Pet. Geol.* 86, 486–498. doi:10.1016/j.marpetgeo.2017.06.009

Wang, W. Y., Pang, X. Q., Chen, Z. X., Dongxia, C., Tianyu, Z., Luo, B., et al. (2019a). Quantitative prediction of oil and gas prospects of the sinian-lower paleozoic in the sichuan basin in central China. *Energy* 174, 861–872. doi:10.1016/j.energy.2019.03.018

Wang, A. G., Wang, Z. L., Li, L., Fan, C. Y., Zhang, K., Xiang, B. L., et al. (2019b). Hydrocarbon migration in the multiple-sourced petroleum system in the northwestern junggar basin (northwestern China): Constraint from geochemical and phase fractionation analysis. *AAPG Bull.* 103, 2247–2284. doi:10.1306/01211916512

Wei, B., Wei, H. H., Chen, Q. H., and Zhao, H. (2003). "Sediment provence analysis of Yanchang Formation in Ordos Basin," in *Journal of northwest university(natural science edition)*, 447–450. (in Chinese with English abstract).

Wu, Z. J., Han, X. Z., Lin, Z. X., Li, Z. N., Ji, H., Yin, D. F., et al. (2020). Tectonic, sedimentary, and climate evolution of meso-cenozoic basins in North China and its significance of coal accumulation and uranium mineralization. *Geotect. Metallogenia* 44, 710–724. (in Chinese with English abstract). doi:10.16539/j.ddgzyckx.2020.04.012

Wu, Z. Q. (2020). *Analysis on the relationship between faults and mesozoic and paleozoic oil and gas reservoirs in Ordos Basin*. M.S. thesis. Xi'an: Northwest University in Xi'an. (in Chinese with English abstract).

Xie, D. L., Yao, S. P., Cao, J., Hu, W. X., Wang, X. L., and Zhu, N. (2021). Diagenetic alteration and geochemical evolution during sandstones bleaching of deep red-bed induced by methane migration in petroliferous basins. *Mar. Pet. Geol.* 127, 104940. doi:10.1016/j.marpetgeo.2021.104940

Xu, Z. J., Liu, L. F., Wang, T. G., Wu, K. J., Dou, W. C., Song, X. P., et al. (2017). Characteristics and controlling factors of lacustrine tight oil reservoirs of the triassic Yanchang Formation Chang 7 in the Ordos Basin, China. *Mar. Pet. Geol.* 82, 265–296. doi:10.1016/j.marpetgeo.2017.02.012

Yang, P., Ren, Z., Zhou, R. J., Cui, J. P., Qi, K., Fu, J. H., et al. (2021). Tectonic evolution and controls on natural gas generation and accumulation in the ordovician system of the Ordos Basin, North China. *Energy Rep.* 7, 6887–6898. doi:10.1016/j.egyr.2021.10.066

Zerda, T., John, A., and Chmura, K. (1981). Raman studies of coals. *Fuel* 60, 375–378. doi:10.1016/0016-2361(81)90272-6

Zhang, L., Liu, C. Y., Zhang, S. H., Fayek, M., Lei, K. Y., and Quan, X. Y. (2022). Unconformity-controlled bleaching of jurassic-triassic sandstones in the Ordos Basin, China. *J. Pet. Sci. Eng.* 211, 110154. doi:10.1016/j.petrol.2022.110154

Zhou, J. G., Yao, G. S., Deng, H. Y., Xin, Y. G., Hu, H., Zheng, X. P., et al. (2008). Exploration potential of Chang 9 member, Yanchang Formation, Ordos Basin. *Pet. explor. Dev.* 35, 289–293. doi:10.1016/S1876-3804(08)60074-9